Prashanthi *et al.*
Micro and Nano Systems Letters (2022) 10:1
https://doi.org/10.1186/s40486-022-00143-w

Micro and Nano Systems Letters

LETTER Open Access

Multiple ratiometric nanothermometry using semiconductor $BiFeO_3$ nanowires and quantitative validation of thermal sensitivity

K. Prashanthi[1*], K. Krishna Mohan[1], Željka Antić[1,2], Kaveh Ahadi[1,3] and Miroslav D. Dramicanin[2]

Abstract

Here, we report a very sensitive, non-contact, ratio-metric, and robust luminescence-based temperature sensing using a combination of conventional photoluminescence (PL) and negative thermal quenching (NTQ) mechanisms of semiconductor $BiFeO_3$ (BFO) nanowires. Using this approach, we have demonstrated the absolute thermal sensitivity of ~ 10 mK^{-1} over the 300–438 K temperature range and the relative sensitivity of 0.75% K^{-1} at 300 K. Further, we have validated thermal sensitivity of BFO nanowires quantitatively using linear regression and analytical hierarchy process (AHP) and found close match with the experimental results. These results indicated that BFO nanowires are excellent candidates for developing high-performance luminescence-based temperature sensors.

Keywords: Temperature sensors, Thermal quenching, Nanowires, Sensitivity validation

Graphical abstract

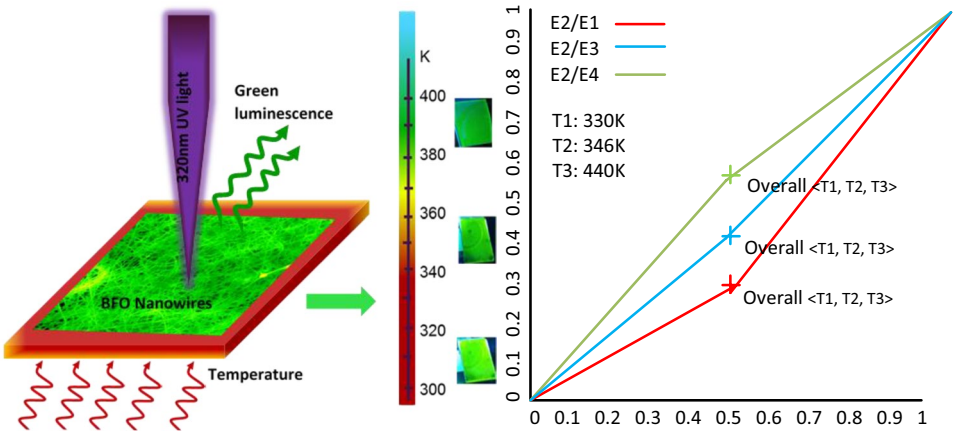

Introduction

A new way of measuring temperature and developing temperature probes is important for applications in emerging environments including nano-biotechnology and integrated optics [1–5]. Currently

*Correspondence: kovur@ualberta.ca
[1] University of Alberta, Edmonton T6G 2V4, Canada
Full list of author information is available at the end of the article

existing temperature measurement technologies or standard thermometers are not able to provide spatial resolution of measurements better than 1 μm, being as such of no use in nanobiotechnology. Further, it is quite difficult to assess inter- or intra-cellular temperature by common thermometers in biological systems. In addition, the ability to remotely detect temperature within the objects volume (unlike from the surface with thermovision camera), lack of interference with electrical current and capability to measure temperature of rotating objects are quite important application, which cannot be easily addressed with conventional methods. Therefore, temperature measurements based on changes in the optical properties of materials can overcome these challenges as they offer non-contact measurements. Among all optical methods, temperature dependencies of the luminescent properties of materials have attracted the most attention due to the sensitivity of luminescence and the ease with which luminescence can be detected in comparison to other optical methods [6–9]. The changes of luminescence properties of nanomaterials with temperature such as changes of absolute and relative emission intensities, lifetime of excited states, emission rise times, peak positions, and emission bandwidths allow them to act as sensitive thermometers. Optical thermometry enables local temperature measurement of a system with submicron spatial resolution [10–12]. Temperature sensing through photoluminescence (PL) is based on the use of either nanoparticles or luminescent molecular probes as it offers a convenient optical measurement method [6, 13, 14]. Recently, the luminescence ratiometric nanothermometry performed via relative emission intensity measurements or luminescence intensity ratios gained a lot of attention because of its self-referencing capability, high precision, and high reliability [15–17]. The ratiometric nanothermometry method is unaffected by the variations in the measurement conditions and changes in the excitation source and can be potentially used in molecular nano thermometers or bioprobes [18–22].

The PL quenching as a function of temperature is strongly associated with the energy difference between transition states and offers high sensitivity in temperature sensing [23–25]. Previous studies on ratiometric thermometry were mainly focussed on conventional thermal quenching of semiconductor materials or other nanophosphors where the emission intensities decrease with increase in tempearture [16, 26, 27]. Such PL quenching mechanism in semiconductors is mainly attributed to the delocalization of charge carriers and consequent trapping by non-radiative centers or energy states (with increasing temperature) which would result in decrease in the number of the charge carriers transitioning from the final energy levels to the initial energy levels. Unlike the conventional thermal quenching in most semiconductors, the negative thermal quenching (NTQ) is the phenomenon where the number of charge carriers transitioning between final and initial energy states increase with increase in temperature. This NTQ behaviour in nanoscale semiconductors is mainly due to the characteristic surface states caused by lattice defects which are responsible for releasing trapped charge carriers in the recombination process at high temperatures. In our recent work, we have demonstrated that the semiconductor BFO nanowires show a rare phenomenon of NTQ of emission [28], where emission intensity of certain peaks as a function of temperature shows an increase in luminescence intensity instead of generally observed trend of decrease in intensity. As reported in [28], the emission associated with an energy state of lower activate energy will not affect their emission characteristics of carriers with increase in temperature. On the contrary, the carriers associated with higher activation energy will gain sufficient energy at higher temperatures, the temperature change affects this emission much more. This anomalous NTQ behavior of BFO nanowires was explained using a multi-level model developed by Shibata [29]. The temperature dependent PL intensity and a very long lifetime of $\sim$ 160 μs was attributed to the trapping and releasing process of the carriers from surface states. In continuation of our published work [28], here, we report on a new way of monitoring temperature variations via NTQ mechanism of BFO nanowires. The multiple ratiometric temperature sensing using a combination of conventional and unconventional (NTQ effect) mechanism offers a promising strategy towards ultrahigh relative sensitivity probing of temperature. Further, we have adopted analytical hierarchy process (AHP) method to validate and strengthen our experimental data.

Experimental procedure

The preparation, structural, optical, and electrical properties characterization of semiconductor BFO nanowires were published by us previously [28, 30–33]. The temperature sensing via luminescence thermometry was performed using a Fluorolog-3 Model FL3-221 spectrofluorometer system (Horiba–Jobin–Yvon) over the temperature range 300–438 K. For temperature dependent PL studies, the BFO nanowires were deposited both on Pt coated Si ($Si/SiO_2/Ti/Pt$) and quartz substrates. The PL measurements were performed under continuous excitation from a 450 W xenon lamp at a wavelength of 320 nm (3.87 eV). The BFO nanowire samples were placed on a custom-made temperature-controlled platform, and emission spectra were collected via an optical fiber bundle. We have used time-resolved photoluminescence to determine

an effective lifetime of minority charge carriers in BFO nanowires as a function of temperature. The temperature dependent time-resolved PL measurements were acquired utilizing a Xenon–Mercury pulsed lamp as excitation source. The temperature of the BFO nanowire sample was controlled by a temperature control system within the accuracy of ± 0.5 K (please refer to the manufacturer's link to get the product details http://microptik.online/190%d1%81-to-400%d1%81/mhcs400/) employing PID (proportional-integral-derivative) feedback loop equipped with a T-type thermocouple for temperature monitoring. The schematic of the experimental setup used for optical (luminescence) thermometry is shown in Fig. 1. The topography imaging of BFO nanowires on quartz substrate was done using atomic force microscopy (AFM) (Bruker Dimension Icon, USA). The ex-situ ellipsometric spectra (Ψ, Δ) were collected using a J. A. Woollam M2000DI at 70° angle of incidence under 400 mTorr vacuum at 325 K, 375 K, 425 K, 375 K, 525 K, and 575 K.

Results and discussions

Temperature dependent optical response

The PL spectra obtained for BFO nanowires at 300 K and at 438 K are presented in Fig. 2a for comparison. The four emission bands with maxima at 2.55 eV (E1), 2.35 eV (E2), 2.27 eV (E3) and 2.23 eV (E4) correspond to the band edge/near band emission (NBE) and defect level/surface state emission (DLE) as reported in our recent work [28]. Inset of Fig. 2a shows room temperature excitation spectrum obtained for BFO nanowires. Figure 2b presents PL spectra of BFO nanowires for E2 defect emission measured in the temperature range of 300–438 K. The PL emission intensity for E2 emission increases with temperatures. Figure 2c shows the evolution of temperature-dependent PL intensity of BFO

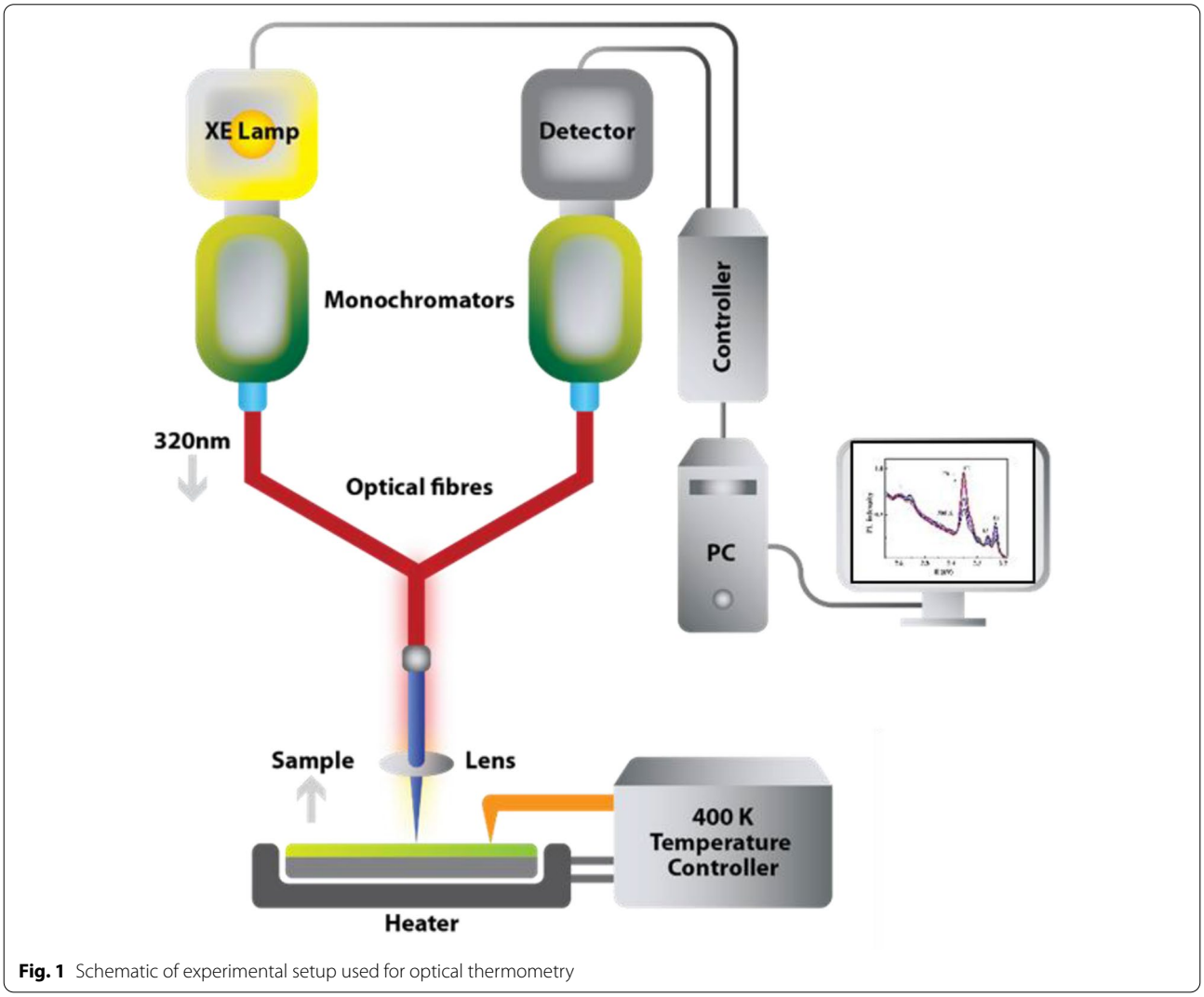

Fig. 1 Schematic of experimental setup used for optical thermometry

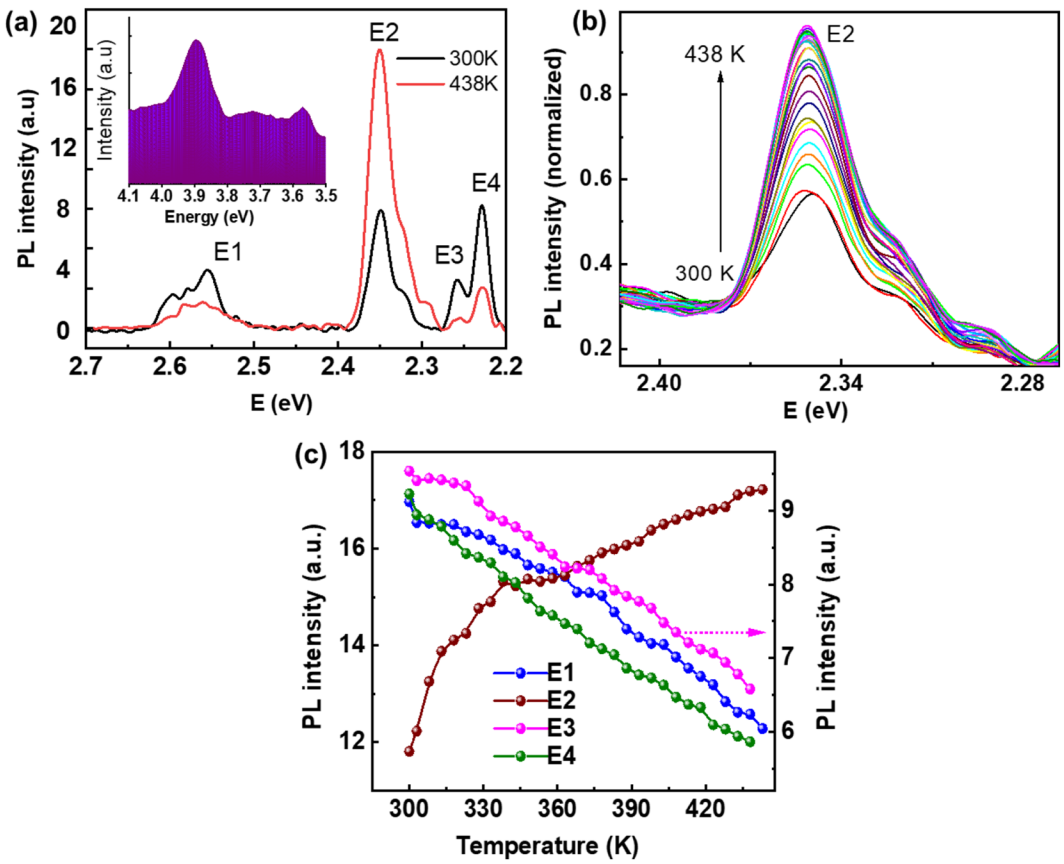

Fig. 2 **a** PL spectra of BFO nanowires for E1, E2, E3, E4 emissions at 300 K and at 438 K. The spectrum shows increase in luminescence intensity with increase in temperature for 2.35 eV (E2) emission, whereas decrease in PL intensity with temperature is observed for other emissions (E1, E3 and E4) (ref. [21]). Inset of **a** shows room temperature excitation spectrum showing a peak at 3.8745 eV (**b**) PL spectra of BFO nanowires for E2 emission over the temperature range of 300–438 K. **c** Intensity of PL spectra plotted as a function of temperature for E1, E2, E3, and E4 emissions. Luminescence intensity increases with an increase in temperature for 2.35 eV (E2) emission, whereas a decrease in PL intensity with temperature is observed for other emissions (E1, E3 and E4)

nanowires for all 4 emissions (E1, E2, E3, and E4) measured at temperatures in the range of 300–438 K. As we can see from Fig. 2c that the PL intensity decreases for E1, E3, and E4 emissions, however, PL intensity increases for E2 emission. Since BFO nanowires provide multiple emission peaks, a ratiometric approach to luminescence thermometry could be used. Since the intensity ratio between two emission bands is calculated from the same measurement, luminescence intensity ratio (LIR) method eliminates errors inherent to temperature readout from the intensity of a single emission band which are caused by fluctuations in excitation intensity or detection system and nonhomogeneous distribution of the probe on the measurement surface and therefore, act as self-referencing (i.e., measurements do not have to be referenced with any temperature standard) [10, 34, 35]. When BFO nanowires are excited with UV light, the photons cause electrons to move into allowed excited states. However, when these electrons return to their equilibrium states, the excess energy is released as photon emission via radiative transition. In our previous work, we have reported that the presence of excess surface states in the band gap of BFO nanowires play an intermediate role during the emission process by capturing the excited carriers and acting as radiation centers with enhanced emission [28]. The increase in temperature results in the release carriers from these surface states and when these carriers again recombine radiatively, they contribute to the green emission.

Figure 3a presents optical images of BFO nanowire samples under the sunlight (300 K) and under UV ($\lambda_{lamp} = 254$ nm) illumination (300 K, 330 K, and 360 K). From the optical images, it can be observed that the BFO nanowires emit green luminescence in the presence of UV light and the intensity of green luminescence decreases as the temperature of the sample is increased from 300 to 360 K. Figure 3b demonstrates an optical transparency of BFO nanowires (deposited on the quartz

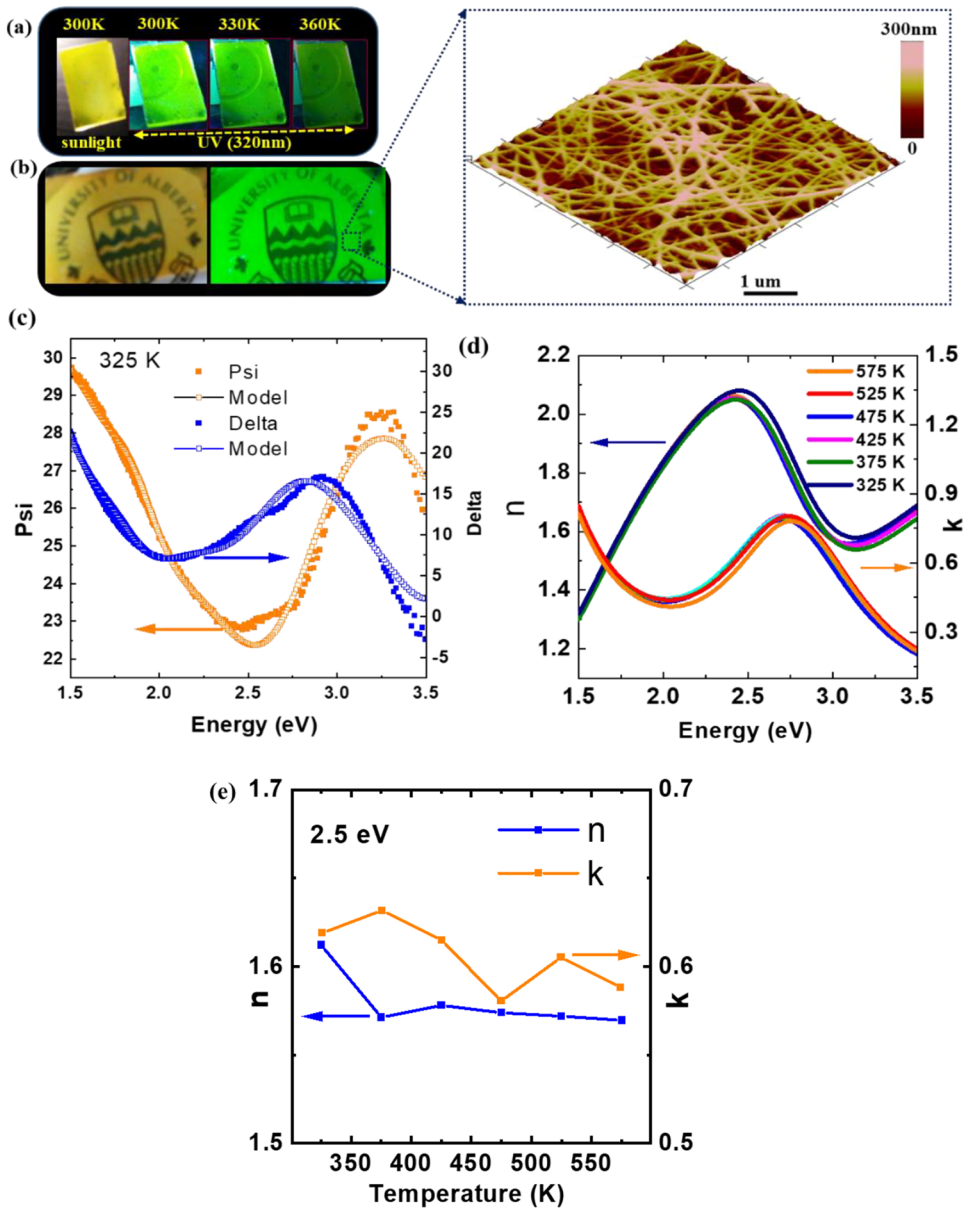

Fig. 3 **a** Optical images of BFO nanowire samples under the sunlight (300 K) and under UV ($\lambda_{lamp} = 254$ nm) illumination (300 K, 330 K, and 360 K). **b** Optical transparency of BFO nanowires under sunlight and under UV illumination ($\lambda_{lamp} = 254$ nm) at 300 K. Enlarged image shows an AFM image of BFO nanowires. **c** The raw Psi and Delta measured by ellipsometry and fitted optical model. The real and imaginary component of refractive index with respect to (**d**) incident photon energy (325 K, 375 K, 425 K, 375 K, 525 K, and 575 K) and (**e**) temperature (at 2.5 eV)

substrate) under sunlight and under UV illumination at 300 K. Our Institutions' logo is clearly seen under the ambient sunlight as well as under UV light demonstrating BFO nanowires have good transparency. Moreover, under UV light excitation, beside good transparency, the green photoluminescence from nanowires is clearly visible. The enlarged portion of Fig. 3b shows an AFM image of BFO nanowires. As demonstrated by the AFM topography, high density of nanowires was achieved on the quartz substrate. Generally, the nanowires have a diameter distribution of 90–250 nm with an average length of tens of micrometers. Further, we have investigated the temperature dependent refractive index (n) and extinction coefficient (k) of BFO nanowires using ellipsometry. The ellipsometric spectra of BFO nanowires were evaluated using the Cauchy model for the quartz substrates. A three-medium optical model consisting of substrate/bulk film/ambient was employed. The optical response of the

BFO nanowires is described by a Tauc-Lorentz oscillator in the band gap energy region [36, 37]. The Bruggeman Effective Medium Approximation (EMA) was employed to count for the voids between the BFO nanowires. Eventually, substrate back side correction was included. Parameters of Tauc-Lorentz oscillators were fitted with least squares regression analysis leading to low mean square error (< 10). Figure 3c reveals the Psi and Delta with an optical model for BFO nanowires. Parameters of Tauc-Lorentz oscillators were fitted with least squares regression analysis leading to low mean square error (< 10). Figure 3d shows the extracted refractive index (n) and extinction coefficient (k) for BFO nanowires, accordingly. The sub-bandgap extinction coefficient (k) for BFO nanowires can be due to the contribution from surface states. Extracted refractive index (n) values agree with ones found in the literature [38]. The refractive index and extinction coefficient data as a function of temperature reveals very useful conclusions. In our study, both the refractive index and extinction coefficient are insensitive to temperature which implies that the band gap not changing with temperature in this range. Both the extracted refractive index and extinction coefficient seem to be insensitive to temperature (Fig. 3e). Usually, a drastic change in refractive index and extinction coefficient is only expected if we have a phase transition. The temperature independent refractive index and extinction coefficient data suggests and help us to conclude that there is no phase transition happening at higher temperature. Furthermore, band gap also qualitatively does not show a drastic change with temperature in this range.

Temperature dependent luminescence decay lifetime

The calculated lifetime values of BFO nanowires as a function of temperature for E2 emission is presented in Fig. 4. The error bars in Fig. 4 represent the mean with 4 experimental trials of a data set. As observed from temperature dependant luminescence lifetime studies, the decay time is ~ 160 µs. Such high decay time is expected because the transitions from surface states are forbidden, which results in slow emission rate. This fluorescence decay time of carries does not really signify the sensor response time, rather it signifies the carrier lifetime. In our previous studies, we have calculated the rise time and fall time for carriers in BFO nanowires and found the rise time and decay time constants are about 70 µs and 190 µs, respectively [32]. The carrier lifetimes obtained for BFO nanowires are very high as compared to that of the reported values in bulk or thin films [39, 40]. Usually for a non-passivated surface, the PL decay time decreases more rapidly with increasing temperature. The temperature dependence of carrier lifetimes also

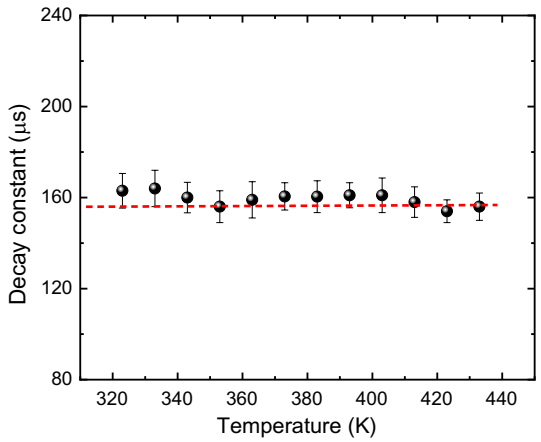

Fig. 4 Lifetime values of BFO nanowires obtained for E2 emission as a function of temperature. The error bars represent the mean with 4 experimental trials of a data set

depends on the surface recombination velocities [41]. In our case, the carrier lifetime shows only a minor or almost no temperature dependence. This temperature independence is due to less recombination or higher surface recombination velocities. The obtained temperature dependent luminescence lifetime value of ~ 160 µs is close to other luminescence thermometry-based temperature sensors [16, 42, 43]. Further, it can be noted from Fig. 4 that the lifetime is independent of the temperature change, resembling the static quenching behavior and can be explained in terms of multiple trapping and de-trapping process as explained in our earlier work [28].

Thermal sensitivity analysis

Figure 5a shows a plot of the temperature dependence of the LIR obtained as ratios of E2 emission with other three (E1, E3 and E4). In principle, for the ratiometric sensing, no knowledge regarding the physics underlying the temperature quenching is needed. It is sufficient to approximate the experimental data for further use as a calibration curve [44]. For the case of BFO nanowires, LIR data are fitted with the linear function as shown in Fig. 5b, and fitting parameters are given in the Table 1. The most important Figures of merits for luminescence thermometry are the absolute sensor sensitivity, S_a defined as the rate at which LIR changes with the temperature, and the relative sensor sensitivity, S_r defined as the normalized absolute sensor sensitivity with respect to the measured value: [10]

$$S_a = \frac{|\partial LIR|}{\partial T}. \quad (1)$$

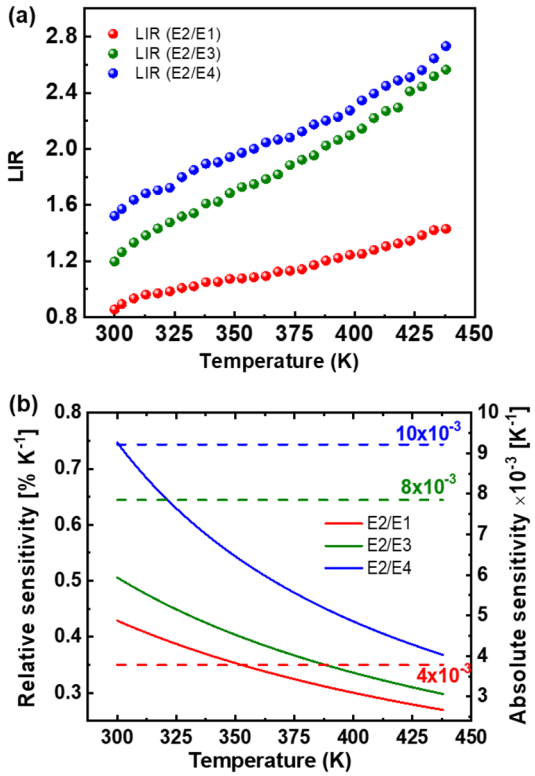

Fig. 5 **a** Luminescence intensity ratio (LIR) values of BFO nanowires as a function of temperature (circles). LIR values were obtained as the ratio between peak intensities for E1, E3, and E4 with respect to E2. **b** Relative and absolute sensor sensitivity obtained from LIR measurements as a function of temperature (300–438 K)

$$S_r = 100\% \times \left| \frac{1}{LIR} \frac{\partial LIR}{\partial T} \right|. \quad (2)$$

The absolute and relative sensitivities of BFO nanowires calculated from Eqs. (1) and (2) are plotted in Fig. 5b and are listed in Table 1. Relative sensitivities achieved with BFO nanowires are similar (slightly lower) but with larger measurement ranges than those reported on ratiometric luminescence thermometry with other semiconductors. However, the observed trend of higher relative sensitivity at lower temperature is in consistent with other reports on ratiometric thermal sensors [9, 16, 45]. Increase in the LIR with increase in temperature in agreement with the argument of transition to the trapped centers before they recombine back radiatively. However, from the relative sensitivity expression, increase in LIR at higher temperatures results decreased relative sensitivity at higher temperatures. Any two energy levels with an energy gap of smaller than 2000 cm^1 are usually denoted by the thermally coupled energy levels and the inter carrier population between which is dominated by the Boltzmann distribution [35, 45–47]. The gradual decrease in Sr with the increase of temperature, suggests that the thermally coupled energy levels show dominance at relatively low temperatures.

Relative sensitivities of 0.9 and 1.3%K^{-1} have been found for differently sized nanoparticles of $Zn_{0.99}Mn_{0.01}Se$/ZnCdSe in the temperature range of 293–373 K [48], and 0.9%K^{-1} with CdSe/ZnSe and CdTe/ZnS over the narrow temperature range of 293–320 K [49]. It should be note that $Zn_{0.99}Mn_{0.01}Se$/ZnCdSe luminescence thermometry has been realized for emission from both semiconductors and Mn^{2+} [10].

Validation of thermal sensitivity using analytical hierarchy process (AHP)

The AHP method deals with linear models (the hierarchy) where the calculations of weights for each LIR and temperature values are based on linear regression to estimate the overall thermal sensitivity of LIR ratio. Therefore, in this paper, we have adopted AHP model to validate and strengthen our experimental data. Based on the data obtained from E2/E4 emission, we have developed intercept equations in $y = a + bx$ form, where y represents dependent variable (relative emission intensity) and x is an independent variable (temperature) through simple linear regression and log value regression. Equation (3) represents linear regression with log value and Eq. (4) represents linear regression with respective evaluated R^2 values. The curve fitting plot and as well equations (with and without log value) with R^2 values are represented in Fig. 6.

Table 1 Table summarizing figure of merits of the luminescence thermometry using negative quenching effect of E2 (2.35 eV) emission of BFO nanowires

LIR ratio	Temperature range	Temperature dependence	Thermal sensitivity	
			S_a (K^{-1})	$S_{r_{max}}$ (% K^{-1}) @ 300 K
E2/E1	300–438 K	$-0.25+0.00378 \cdot T$	4×10^{-3}	0.43
E2/E3	300–438 K	$-0.25+0.00785 \cdot T$	8×10^{-3}	0.51
E2/E4	300–438 K	$-1.53+0.00922 \cdot T$	10×10^{-3}	0.75

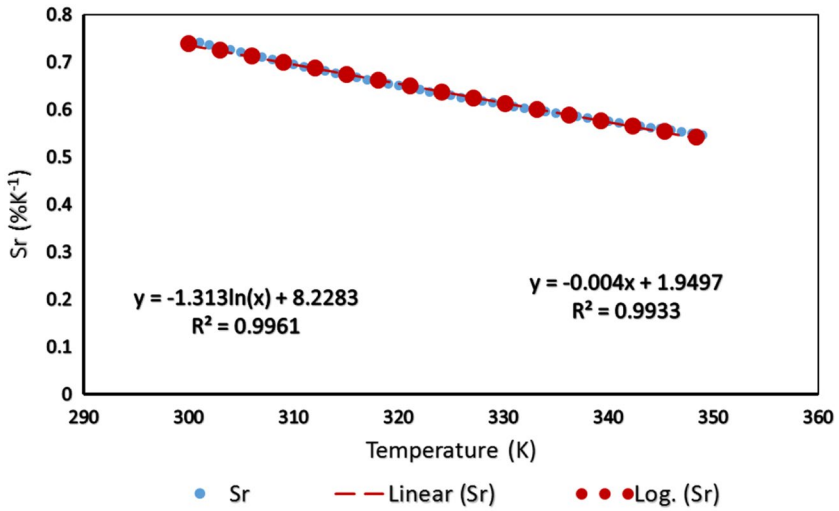

Fig. 6 Prediction of relative sensitivity (S_r) for E2/E4 as a function of temperature (300–438 K) using linear regression

$$y = -1.313\ln(x) + 8.22; R^2 = 0.9961. \quad (3)$$

$$y = -0.004x + 1.94; R^2 = 0.9933. \quad (4)$$

One of the evaluated parameters will help the expert instantly with linear regression is R^2. The statistical significance of R^2 is a degree of how well our considered application is appropriately fitting the actual data close to linearity relationship. The linearity relationship in this case is between temperature and E2/E4 emission intensity. The value of R^2 should always lies between the spectrum of 0–1. If the value is close to 1, then the observed variance of linearity is high and whereas if it is close to 0 then the linear relationship is considered to be weak or low. However, we can predict the target signal in either of the cases with a high or low linearity relationships. In our case the R^2 (log-linear) is calculated to be 0.9961 while in simple linear as 0.9933 (without log). Since, the R^2 value is close to 1, we conclude the relationship of sensitivity with temperature is strongly linear. Since, the regression results are found linear, we have further conducted validation of thermal sensitivity of BFO nanowires using LIR ratios at different temperatures via the AHP model [50–54]. The validation model analysis of thermal sensitivity has been accomplished using AHP quantitatively. The AHP, a prominent methodology founded on multi-criteria decision-making model established by Saaty [51] aims at quantifying influencing factors. In our paper, we have quantified emission intensities at different temperatures, in other words at varying levels of abstraction of temperature sensing using semiconductor BFO nanowires and further observed its sensitive analysis. The quantification is performed through the data obtain from LIR ratios (E2/E1, E2/E3, E2/E4) through a series of experiments. Thus, we translate the acquired data patterns into the scale 1 to 9 (based on the emission intensity) of the AHP model suggested by Saaty [50]. To recall, here, we present a brief classification of steps involved in AHP quantitative evaluation through series of steps: (a) defining the objective of the considered application problem, (b) modeling influencing factors into hierarchy at various appropriate levels, (c) forming pair-wise comparison matrices among the factors at each level of the hierarchy, (d) evaluation of the matrices through weigh vectors via principal Eigen vector [51], (e) pooling of all assessed weigh vectors according to the hierarchy model, and lastly (f) final quantification evaluation and sensitivity analysis [55].

Specifically, in this paper, we have investigated the merits of AHP for quantitative validation of the thermal sensitivity of BFO nanowires and performed the following assessments:

- Quantified and validated thermal sensitivity using LIR ratios (E2/E1, E2/E3, E2/E4) at 300 K.
- Similarly, further quantified LIR ratios at 346 K and 440 K.
- Finally, node sensitivities at each of the LIR ratios w.r.t overall temperature range of 300–440 K.

Thus, we applied steps (a–f) AHP algorithm mentioned above to quantify thermal sensitivity of BFO nanowires using LIR ratios. The first step (a) been defining the objective—the validation of thermal sensitivity of LIR ratios quantitatively. In step (b), based on

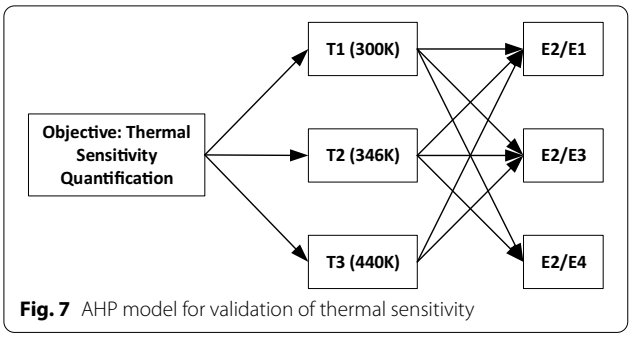

Fig. 7 AHP model for validation of thermal sensitivity

the experimental results for thermal sensitivity of BFO nanowires using LIR ratios at different temperature, we have modelled in a 2 layered hierarchy, shown Fig. 7. The first level consists of considered three temperatures T1 (300 K), T2 (346 K), and T3 (440 K). The second layer and the last level includes LIR ratio (E2/E1, E2/E3, E2/E4).

In the steps (c), formulated pair-wise comparison matrices with one pair matrix at the first level and three pair-wise matrices at the second level. Next in the step (d), assessment of four matrices through weigh vectors evaluations has been performed. The formulation and evaluations of matrices from steps (c) and (d) are shown in the Table 2. All the weight vectors calculated from four matrices in step (d) are pooled and organized via. in the form aggregation matrix shown in the Table 3, this completes the step (e). Finally, in the step (f), we perform concluding evaluation from the aggregation matrix (from

Table 2 Formulation of pair-wise matrices and assessments

Level 1: (a) Relative importance among T1, T2, and T3				
	T1	**T2**	**T3**	**Weigh vector**
T1	1	1/5	1/6	**0.0811**
T2	5	1	1/2	**0.3420**
T3	6	2	1	**0.5769**
Level 2: (b) Variations of LIR (E2/E1, E2/E3,& E2/E4) @ T1(300 K)				
T1	**E2/E1**	**E2/E3**	**E2/E4**	**Weigh vector**
E2/E1	1	1	1/3	**0.2211**
E2/E3	1	1	1	**0.3189**
E2/E4	3	1	1	**0.4599**
Level 2: (c) Variations of LIR (E2/E1, E2/E3,& E2/E4) @ T2 (346 K)				
T2	**E2/E1**	**E2/E3**	**E2/E4**	**Weigh vector**
E2/E1	1	1/3	1/4	**0.1219**
E2/E3	3	1	1/2	**0.3196**
E2/E4	4	2	1	**0.5584**
Level 2: (d) Variations of LIR (E2/E1, E2/E3,& E2/E4) @ T3 (440K)				
T3	**E2/E1**	**E2/E3**	**E2/E4**	**Weigh vector**
E2/E1	1	1/6	1/7	**0.0760**
E2/E3	6	1	1	**0.4527**
E2/E4	7	1	1	**0.4712**

Bold values are the outcome of the individual matrices

Table 3 Aggregation matrix

Temp →	**T1 (300 K)**	**T2 (346 K)**	**T3 (440 K)**	**Evaluation comments**
$A_i \rightarrow$	0.0811 (a_1)	0.3420 (a_2)	0.5769 (a_3)	Relative importance among T1, T2 and T3
LIR ratios ↓	$\mathbf{A_{ij}} \downarrow$			
E2/E1	0.2211 (a_{11})	0.1219 (a_{21})	0.0760 (a_{31})	Variations of LIR (E2/E1, E2/E3 and E2/E4) w.r.t to T1, T2 and T3
E2/E3	0.3189 (a_{12})	0.3196 (a_{22})	0.4527 (a_{32})	
E2/E4	0.4599 (a_{13})	0.5584 (a_{23})	0.4712 (a_{33})	

Table 4 Final evaluation

Let us denote $A^{(1)} = a_1$, $A^{(2)} = a_2$, $A^{(3)} = a_3$
Overall thermal sensitivity of LIR ratio (E2/E1, E2/E3, and E2/E4) over the temperature range of 300–440 K
$= \sum_{k=1}^{3} \left[\sum_{i=1}^{i_k} A_i^{(k)} A_{ij}^{(k)} \right]$; for j = 1, 2, 3; $i_1 = 3$ (in our case)
= 0.1009 (E2/E1)
0.3960 (E2/E3)
0.5029 (E2/E4)

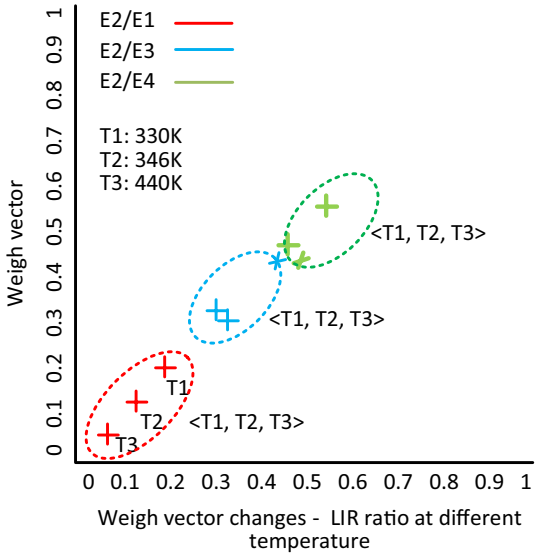

Fig. 8 Sensitivity analysis through clusters LIR ratios at 300 K, 346 K, and 440 K

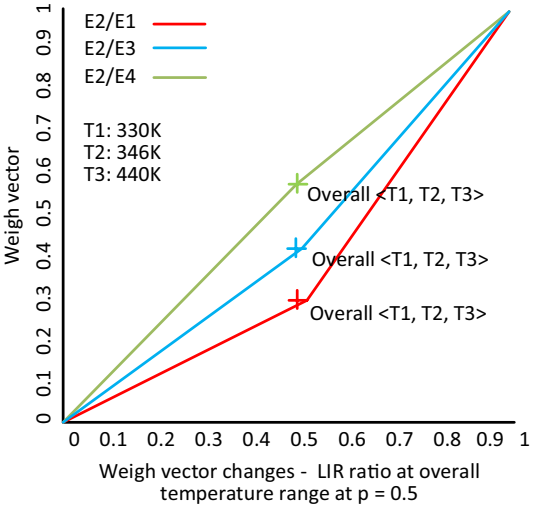

Fig. 9 Node sensitivities of LIR ratios (p = 0.5) at the overall temperature range (300–440 K)

Table 5 Thermal sensitivity validations

	$S_{r\,max}$ (% K^{-1}) @ 300 K (Table 1)		AHP model (Table 2b)
LR values	Ideal values	Normalized	Normalized
E2/E1	0.43	0.254	0.2211
E2/E3	0.51	0.301	0.3189
E2/E4	0.75	0.443	0.4599

step d) through a customized equation to evaluate the overall node sensitivities (at each of the LIR ratios) at the overall temperature range of 300–440 K of the considered application shown in Table 4.

Based on AHP modelling and assessment, we have validated the following pieces of quantitative analysis: (i) Table 2a validated thermal sensitivity using LIR ratios of E2/E1, E2/E3, E2/E4 at 300 K (room temperature); (ii) Similarly, further quantified LIR ratio at 346 K and 440 K, shown in the Table 2b, c; and (iii) Fig. 8 demonstrates sensitivity analysis through clusters LIR ratios at 300 K, 346 K, and 440 K and finally, Fig. 9 depicts the node sensitivities at p = 0.5 (at each of the LIR ratios) at the overall temperature range of 300–440 K.

The ultimate aim of validation of the AHP results is to compare the experimental trend of thermal sensitivity of semiconductor BFO nanowires using LIR ratios. For illustrative purpose, we have compared the results of AHP for LIR ratios of E2/E1, E2/E3, E2/E4) at 300 K with the results of Table 1 and Fig. 5a. We found a close match between AHP model with the simulation result (Table 1) and experimental tendency pattern results in Fig. 5a. The comparison of results obtained from these methods are shown in Table 5. Therefore, our analytical validation results endorse the experimental analysis results of thermal sensitivity of semiconductor BFO nanowires.

Conclusion

Multiple peaks in the emission spectrum of BFO nanowires enabled the use of ratio-metric luminescence temperature sensing in the range of 300–438 K with the relative sensitivity as high as 0.75% K^{-1}. Additionally, using a linear regression and AHP, the quantitative validation has been performed for thermal sensitivity of BFO nanowires using LIR ratios at three different temperatures (300 K, 346 K, and 440 K) and as well at overall temperature range of 300–440 K. In order to demonstrate quantitative validation of the AHP model, we have compared LIR ratio (E2/E1) at room temperature (300 K)

with the experimental results and found a close match. In conclusion, our studies indicate that BFO nanowires can serve as potential candidate for multiple ratiometric nanothermometry based temperature sensors.

Acknowledgements
Authors would like to thank Dr. Thomas Thundat for useful discussions.

Authors' contributions
All the authors contributed for the design of experiments, data analysis, and preparation of the manuscript. All authors read and approved the final manuscript.

Funding
This work was supported by Canada Excellence Research Chairs (CERC) Program and the Serbian Ministry of Education, Science and Technological development (Project Number 17022).

Availability of data and materials
All the data generated and analyzed during this study is included in this manuscript.

Declarations

Ethics approval and consent to participate
Not applicable.

Consent for publication
Not applicable.

Competing interests
The author(s) declare(s) that they have no competing interests.

Author details
[1]University of Alberta, Edmonton T6G 2V4, Canada. [2]University of Belgrade, P.O. Box 522, 11001 Belgrade, Serbia. [3]University of California, Santa Barbara, CA 93106-5050, USA.

Received: 7 September 2021 Accepted: 4 January 2022
Published online: 10 January 2022

References

1. Roriz P, Silva S, Frazão O, Novais S (2020) Optical fiber temperature sensors and their biomedical applications. Sensors (Switzerland) 20:2113
2. Wang F, Han Y, Gu N (2021) Cell temperature measurement for biometabolism monitoring. ACS Sens 6:290–302
3. Sato MK et al (2014) Temperature changes in brown adipocytes detected with a bimaterial microcantilever. Biophys J 106:2458–2464
4. Inomata N, Toda M, Sato M, Ishijima A, Ono T (2012) Pico calorimeter for detection of heat produced in an individual brown fat cell. Appl Phys Lett 100:154104
5. Johnson LM, Leonberger FJ, Pratt GW (1982) Integrated optical temperature sensor. Appl Phys Lett 41:134–136
6. Wang X, Wolfbeis OS, Meier RJ (2013) Luminescent probes and sensors for temperature. Chem Soc Rev 42:7834
7. Marciniak L, Trejgis K, Lisiecki R, Bednarkiewicz A (2020) Synergy between NIR luminescence and thermal emission toward highly sensitive NIR operating emissive thermometry. Sci Rep 10
8. Uchiyama S, Gota C (2017) Luminescent molecular thermometers for the ratiometric sensing of intracellular temperature. Rev Anal Chem 36
9. Getz MN, Nilsen O, Hansen PA (2019) Sensors for optical thermometry based on luminescence from layered YVO4: Ln^{3+} (Ln = Nd, Sm, Eu, Dy, Ho, Er, Tm, Yb) thin films made by atomic layer deposition. Sci Rep 9
10. Brites CDS et al (2012) Thermometry at the nanoscale. Nanoscale 4:4799
11. Vetrone F et al (2010) Temperature sensing using fluorescent nanothermometers. ACS Nano 4:3254–3258
12. Jaque D, Vetrone F (2012) Luminescence nanothermometry. Nanoscale 4:4301
13. Garcia DJ, Sole JG (2016) Thermometry at the nanoscale: techniques and selected applications. In: Carlos LD, Palacio F (eds) RSC nanoscience and nanotechnology, vol 38. The Royal Society of Chemistry, UK, pp 83–123
14. Wang S, Westcott S, Chen W (2002) Nanoparticle luminescence thermometry. J Phys Chem B 106:11203–11209
15. Dramićanin MD, Antić Ž, Ćulubrk S, Ahrenkiel SP, Nedeljković JM (2014) Self-referenced luminescence thermometry with Sm^{3+} doped TiO_2 nanoparticles. Nanotechnology 25:485501
16. Antić Ž et al (2016) Pulsed laser deposited dysprosium-doped gadolinium-vanadate thin films for noncontact. Self-referencing luminescence thermometry. Adv Mater 28:7745–7752
17. Lojpur V, Ćulubrk S, Dramićanin MD (2015) Ratiometric luminescence thermometry with different combinations of emissions from Eu^{3+} doped $Gd_2Ti_2O_7$ nanoparticles. J Luminesc 169:534–538. https://doi.org/10.1016/j.jlumin.2015.01.027
18. Kamimura M, Matsumoto T, Suyari S, Umezawa M, Soga K (2017) Ratiometric near-infrared fluorescence nanothermometry in the OTN-NIR (NIR II/III) biological window based on rare-earth doped β-NaYF4 nanoparticles. J Mater Chem B 5:1917–1925
19. Dong N-N et al (2011) NIR-to-NIR two-photon excited CaF_2:Tm^{3+}, Yb^{3+} nanoparticles: multifunctional nanoprobes for highly penetrating fluorescence bio-imaging. ACS Nano 5:8665–8671
20. Smith AM, Mancini MC, Nie S (2009) Bioimaging: second window for in vivo imaging. Nat Nanotechnol 4:710–711
21. Jaque D et al (2016) Inorganic nanoparticles for optical bioimaging. Adv Opt Photon 8:1–103
22. Hemmer E, Benayas A, Légaré F, Vetrone F (2016) Exploiting the biological windows: current perspectives on fluorescent bioprobes emitting above 1000 nm. Nanoscale Horizons 1:168–184
23. Paje SE, Llopis J (1992) Temperature dependence of the photoluminescence and phosphorescence time decay of magnesia-stabilized zirconia. Appl Phys Solid Surf 55:523–528
24. Fang Y-C, Chu S-Y, Kao P-C, Chuang Y-M, Zeng Z-L (2011) Energy transfer and thermal quenching behaviors of CaLa[sub 2](MoO[sub 4])[sub 4]:Sm[sup 3+], Eu[sup 3+] red phosphors. J Electrochem Soc 158:J1
25. Đačanin LJR, Lukić-Petrović SR, Petrović DM, Nikolić MG, Dramićanin MD (2014) Temperature quenching of luminescence emission in Eu^{3+}- and Sm^{3+}-doped $YNbO_4$ powders. J Luminesc 151:82–87
26. Lojpur V et al (2013) Luminescence thermometry with Zn_2SiO_4:Mn_2 powder. Appl Phys Lett 103:2013–2016
27. Yu H, Su W, Chen L, Deng D, Xu S (2019) Excellent temperature sensing characteristics of europium ions self-reduction $Sr_3P_4O_{13}$ phosphors for ratiometric luminescence thermometer. J Alloy Compd 806:833–840
28. Prashanthi K, Antić Ž, Thakur G, Dramićanin MD, Thundat T (2018) Surface state-induced anomalous negative thermal quenching of multiferroic $BiFeO_3$ nanowires. Phys Status Solidi Rapid Res Lett 12:1–6
29. Shibata H (1998) Negative thermal quenching curves in photoluminescence of solids. Japan J Appl Phys Part 1 Regular Papers Short Notes Rev Papers 37:550–553
30. Prashanthi K, Thakur G, Thundat T (2012) Surface enhanced strong visible photoluminescence from one-dimensional multiferroic $BiFeO_3$ nanostructures. Surf Sci 606:L83–L86
31. Prashanthi K, Gaikwad R, Thundat T (2013) Surface dominant photoresponse of multiferroic $BiFeO_3$ nanowires under sub-bandgap illumination. Nanotechnology 24:505710
32. Prashanthi K et al (2015) Enhanced photo-collection in single $BiFeO_3$ nanowire due to carrier separation from radial surface field. Nano Energy 13:240–248
33. Prashanthi K, Phani A, Thundat T (2015) Photothermal electrical resonance spectroscopy of physisorbed molecules on a nanowire resonator. Nano Lett 15:5658–5663
34. Gavrilović TV, Jovanović DJ, Lojpur V, Dramićanin MD (2014) Multifunctional Eu^{3+}- and Er^{3+}/Yb^{3+}-doped $GdVO_4$ nanoparticles synthesized by reverse micelle method. Sci Rep 4:1–9
35. Wade SA, Collins SF, Baxter GW (2003) Fluorescence intensity ratio technique for optical fiber point temperature sensing. J Appl Phys 94:4743–4756

36. Ahadi K, Cadien K (2016) RSC Advances Ultra low density of interfacial traps with mixed thermal and plasma enhanced ALD of high- k gate. RSC Adv 6:16301–16307
37. Anti Ž et al (2017) Transparent and highly luminescent dysprosium-doped $GdVO_4$ thin films fabricated by pulsed laser deposition. Thin Solid Films 638:332–337
38. Ihlefeld JF et al (2008) Optical band gap of $BiFeO_3$ grown by molecular-beam epitaxy. Appl Phys Lett 92:140928. https://doi.org/10.1063/1.2901160
39. Zang Y et al (2012) Investigation of the improved performance in a graphene/polycrystalline $BiFeO_3$/Pt photovoltaic heterojunction: experiment, modeling, and application. J Appl Phys 112:054103
40. Sheu YM et al (2012) Ultrafast carrier dynamics and radiative recombination in multiferroic $BiFeO_3$. Appl Phys Lett 100:242904
41. Weiss TP et al (2019) Time-resolved photoluminescence on double graded Cu(In, Ga)Se_2—impact of front surface recombination and its temperature dependence. Sci Technol Adv Mater 20:313–323
42. Li L, Qin F, Zheng Y, Zhang Z (2019) Strategy for highly sensitive optical ratiometric temperature measurement. Opt Mater Express 9:3260
43. Hernández-Rodríguez MA et al (2021) 1000 K optical ratiometric thermometer based on Er^{3+} luminescence in yttrium gallium garnet. J Alloys Compounds 886:161188
44. Nikolić MG, Antić Ž, Ćulubrk S, Nedeljković JM, Dramićanin MD (2014) Temperature sensing with Eu^{3+} doped TiO_2 nanoparticles. Sens Actuators B Chem 201:46–50
45. Li L et al (2018) Relative sensitivity variation law in the field of fluorescence intensity ratio thermometry. Opt Lett 43:186
46. Wang X et al (2015) Optical temperature sensing of rare-earth ion doped phosphors. RSC Adv 5:86219–86236
47. Rai VK (2007) Temperature sensors and optical sensors. Appl Phys B Lasers Opt 88:297–303
48. Vlaskin VA, Janssen N, van Rijssel J, Beaulac R, Gamelin DR (2010) Tunable dual emission in doped semiconductor nanocrystals. Nano Lett 10:3670–3674
49. Jorge P, Martins MA, Trindade T, Santos JL, Farahi F (2007) Optical fiber sensing using quantum dots. Sensors 7:3489–3534
50. Wind Y, Saaty TL (1980) Marketing applications of the analytic hierarchy process. Manage Sci 26:641–658
51. Saaty TL (2003) Decision-making with the AHP: why is the principal eigenvector necessary. Eur J Opera Res 145:85–91
52. Mohan KK, Prashanthi K, Hull R, Montemagno CD (2018) Risk assessment of a multiplexed carbon nanotube network biosensor. IEEE Sens J 18:4517–4528
53. Mohan KK, Reformat MZ, Pedrycz W (2012) Analytic hierarchy process and granularity: assessment of risk severity on livestock wellness. In: 2012 Annual Meeting of the North American Fuzzy Information Processing Society, NAFIPS 2012 (IEEE, 2012). https://doi.org/10.1109/NAFIPS.2012.6291021
54. Mohan KK, Reformat MZ, Pedrycz W (2012) Assessment of risk severity on livestock wellness
55. Chang C, Wu C, Lin C, Chen H (2007) An application of AHP and sensitivity analysis for selecting the best slicing machine. Comput Indus Eng 52:296–307

Publisher's Note